Energy Transfer Via Exciton Transport in Quantum Dot Based Self-Assembled Fractal Structures

César Bernardo[§], Isabel Moura[§*], Y. Núnez Fernández[+], Eduardo J. Nunes-Pereira[§],

Paulo J. G. Coutinho[§], Arlindo M. Fontes Garcia[§], Peter Schellenberg[§], Michael

Belsley[§], Manuel F. Costa[§], Tobias Stauber[φ], and Mikhail Vasilevskiy[§]

[§] Centro de Física, Universidade do Minho, Campus de Gualtar, Braga, Portugal

[+] Centro Atómico Bariloche, CONICET, 8400 Bariloche, Argentina

[φ] Departamento de Física de la Materia Condensada, Universidad Autónoma de Madrid,

Madrid, Spain

[*]E-mail: mouraisabel1@gmail.com, Tel: 00351-253604060, Fax: 00351-253604061

Supplementary Material

1. Autocorrelation function of dendrite images

The autocorrelation function of the microscopic images of the structures is defined as

$$ACF(x,y) = \frac{\int_A Z(x',y')Z(x+x',y+y')dx'dy'}{\int_A Z^2(x',y')dx'dy'} \quad , \tag{S1}$$

where $Z(x,y)$ is the gray scale variable varying between 0 and 255. We assume that
ACF mimics the density-density correlation function. Within a certain range of
$r = \sqrt{x^2 + y^2}$, the latter is expected to decrease with r according to a power law for
known fractal structures (43). ACF plots of our dendrites are shown in figure S1.

At small distances from the center, ACF indeed decreases with r according to r^{D-2},
where D is the Hausdorff dimension of the structure. However, it drops more abruptly
at higher distances approaching the edges of the fractal structure. The effective size is
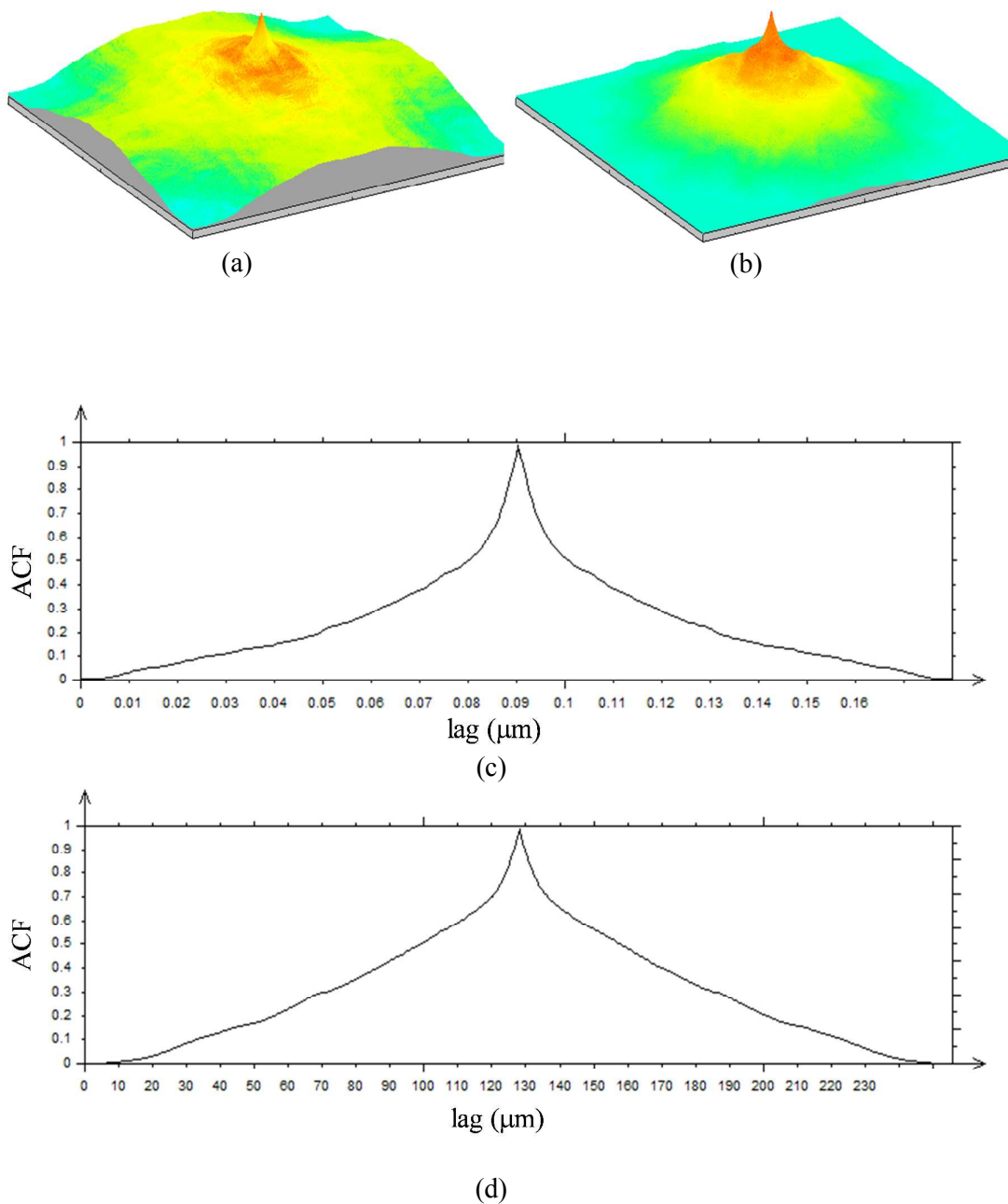given in the figure caption.

(a)

(b)

lag (μm)

(c)

lag (μm)

(d)

Figure S1. Autocorrelation function of microscopic images of CdSe/ZnS (a, c) and CdTe (b, d) dendrites shown in Fig. 4 of the article. The two-dimensional profiles (c) and (d) correspond to some arbitrarily chosen directions in the (*x,y*) plane of the 3D relief maps (a) and (b). The correlation length is $32.0 \pm 1.2 \, \mu m$ and $49.6 \pm 1.6 \, \mu m$ for the structures (a) and (b), respectively.

2. Spectral dependence of the PL decay kinetics

Figure S2 demonstrates the dependence of the PL decay kinetics upon detection

wavelength within the QD emission band. In this case of CdSe/ZnS dots, the fluorescence decay time estimated by a monoexponential fit increases by a factor of 2.5 when changing the detection wavelength from 515 nm to 590 nm. In contrast, for CdTe NCs the characteristic decay time only slightly depends on the detection wavelength, as depicted in Fig. S2 (b).
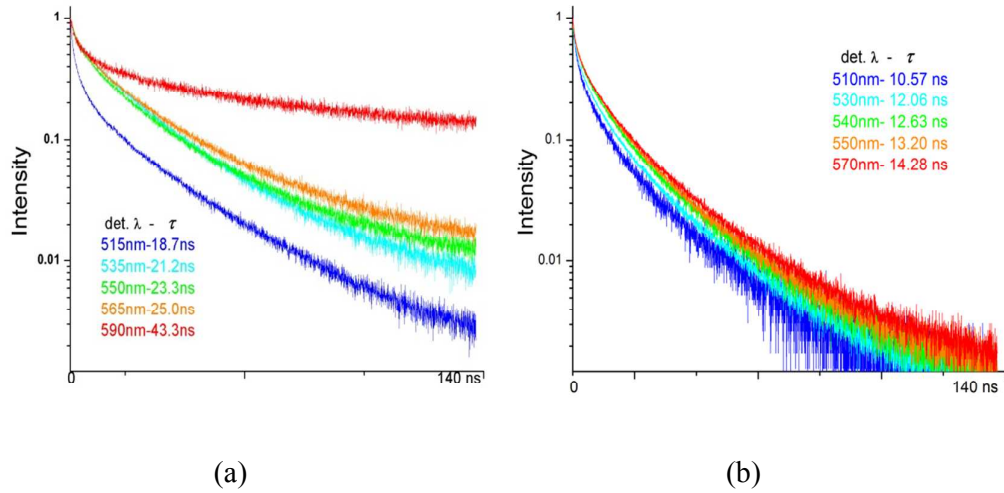

(a)   (b)

Figure S2. Fluorescence decay in CdSe/ZnS (a) and CdTe (b) QDs dissolved in water, measured at different emission wavelengths. Excitation was at 400 nm in all cases.

3. Additional data on FLIM maps

We also checked how the FLIM maps depend on the detection wavelength. As it can be seen from Fig. S3, the maps are qualitatively similar for three different detection wavelengths within the emission spectrum of CdTe QDs.
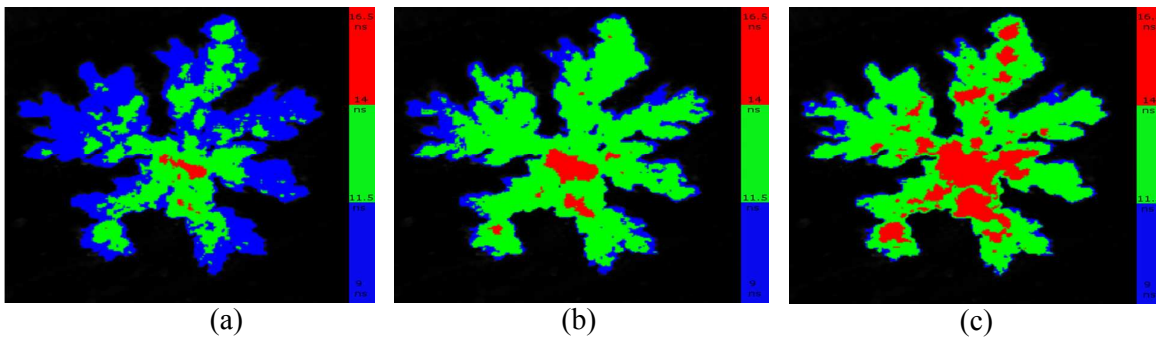

(a)   (b)   (c)

Figure S3. Maps of the average lifetime for a CdTe fractal structure: the wavelength of excitation was 400 nm and emission acquired at (a) 530 nm, (b) 545 nm and (c) 560 nm.

Another issue is the spatial distribution of the decay rate PDF (or its moments). To investigate this, we performed a multiexponential fit of the decay kinetics measured at different points of the dendrite and created a map (Fig. S4) showing the spatial distribution of the normalized decay amplitude (A_1) of the dominant decay component (if the decay were a monoexponential, we would have $A_1 = 1$). In Fig. S4 the relative contribution of the most characteristic decay rate, A_1, is between 65 and 70 % showing no significant inhomogeneity.
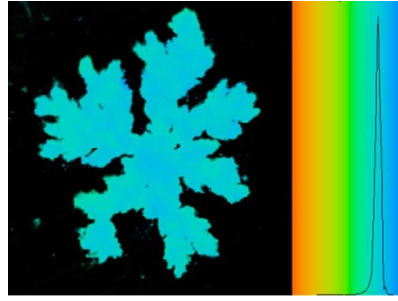

Figure S4. Map of the relative weight of the dominant decay rate.

4. Calculated fluorescence intensity maps
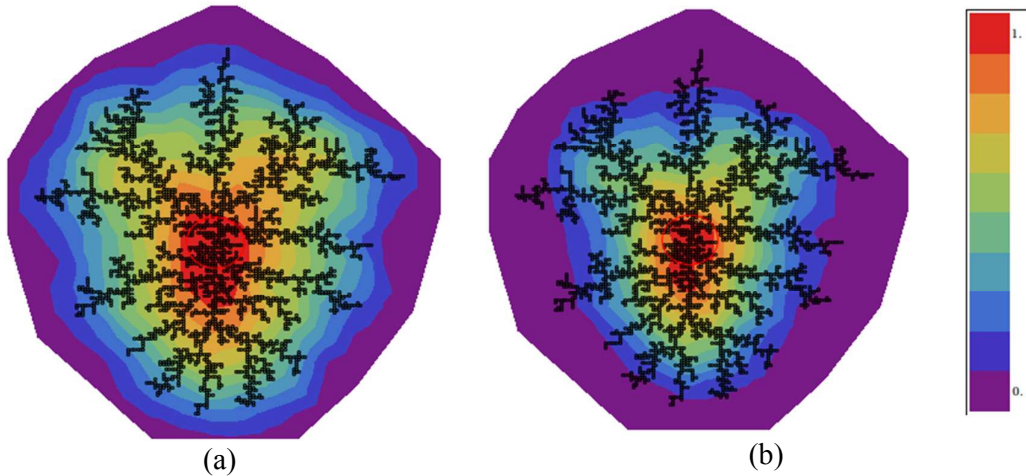

(a)   (b)

Figure S5. Calculated fluorescence intensity maps for generated DLA fractal clusters of monosize QDs, for two values of the Förster radius (expressed in units of the QD radius): (a) $R_F/R = 1$, (b) $R_F/R = 5$. The corresponding FLIM maps are presented in Fig. 7 of the main text.